Journal of Photochemistry & Photobiology, A: Chemistry 450 (2024) 115420

Contents lists available at ScienceDirect

Journal of Photochemistry & Photobiology, A: Chemistry

journal homepage: www.elsevier.com/locate/jphotochem

Self-cleaning and UV-blocking cotton – Fabricating effective ZnO structures for photocatalysis

Alicja Lawrynowicz *, Emilia Palo, Rustem Nizamov, Kati Miettunen

Department of Mechanical and Materials Engineering, University of Turku, FI-20014 Turku, Finland

ARTICLE INFO

Keywords:
ZnO
Cotton
Advanced textiles
Self-cleaning
Photocatalysis
UV blocking

ABSTRACT

This study comprehensively examines the relationship between synthesis conditions that affect the morphologies of ZnO crystals and, therefore, the resulting properties of ZnO-coated self-cleaning and UV blocking textiles. Although the current literature presents several individual recipes, this study uniquely identifies and documents the impact of different processing methods and additives on crystal morphology within one complete synthesis protocol—that is, NaOH concentration, microwaving duration, and NH_4OH additive quantity. Consequently, we suggest a simple and surfactant-free microwave-assisted method of forming ZnO coating with a distinctive flower-like morphology and high surface coverage, with demonstrated optimal self-cleaning performance: a solution of 66 ml of 0.1 M NaOH, 33 ml of 0.2 M of ZnAc dissolved in EtOH, and 2 ml of NH_4OH microwaved for 5 min. The efficacy of ZnO-coated cotton in ultraviolet (UV) blocking was verified with UV protection factor calculations, reaching a near-complete UV blocking capability (as high as 99.93 % for UV-B). The evaluation of photocatalytic self-cleaning performance involved monitoring the discoloration of coffee and methylene blue (MB) stains under 1 Sun, using the innovative photo analysis-based method. The MB dye degradation efficiency of the best-performing samples reached 73 % within the first hour of 1 sun exposure, which is double the speed reported in related studies. The results confirm that flower-like ZnO coating, produced through our simplified protocol, is a viable option for the development of UV-resistant and self-cleaning textiles.

1. Introduction

Cotton, a globally utilized textile fabric, is valued for its breathability, comfort, and high moisture absorbency. However, the valued moisture absorbance, which comes from the high presence of hydroxyl groups on the cotton's surface, makes cotton prone to staining [1,2]. Multiple methods can be employed to enhance the surface properties of cotton, including so-called self-cleaning coatings [3]. These coatings have demonstrated the ability to significantly boost stain repellent properties while preserving the softness of cotton and ensuring user comfort [4,5].

In recent years, research on functional textiles has focused on self-cleaning coatings achieved through hydrophobic and/or photocatalysis approaches [6,7]. Especially attractive are self-cleaning coatings made of metal oxides, such as TiO_2 and ZnO, since they are cheap, easily accessible, and efficient to fabricate [1,8–11]. Both materials offer excellent photocatalysis-based self-cleaning that utilizes light-activated mechanisms to break down organic contaminants, such as microbes and pollutants [12–20]. Both materials can perform well in medical, space, or military applications [10,15,21], where hygiene is particularly important due to the surrounding requirements. Interestingly, the photocatalytic degradation of pollutants has been considered the most effective and sustainable self-cleaning method for textiles [22]. This environmental aspect must be highlighted, as photocatalytic coatings on textiles can result in a substantial reduction of water consumption [9,23,24].

Although TiO_2 remains the most popular photocatalyst in multifunctional commercially available products, ZnO is also regarded as a highly promising alternative due to its exceptional physiochemical properties [25,26], including biocompatibility, biodegradability, high photostability, absorption of a broad range of radiation, and low toxicity [27–33]. Further, similar to TiO_2, nano-sized ZnO absorbs light in the ultraviolet (UV)-A and UV-B regions of spectra; thus, it can serve as a blocker of UV irradiation. Furthermore, ZnO structures arranged in a thin layer can be more flexible than TiO_2 structures [34]. Thus, compared with TiO_2, ZnO could be regarded as a more suitable candidate for textile-based substrates.

The properties of ZnO are profoundly dependent on the size and

* Corresponding author.
E-mail address: alicja.lawrynowicz@utu.fi (A. Lawrynowicz).

https://doi.org/10.1016/j.jphotochem.2023.115420
Received 29 September 2023; Received in revised form 30 November 2023; Accepted 14 December 2023
Available online 20 December 2023

shape of its nanostructures [35]. Since the morphology of ZnO is strongly affected by the parameters of the synthesis process, there is a need to develop and improve methods for the controlled growth of ZnO crystals, especially when ZnO is grown directly on the textile substrate [28]. Based on the desired applications, research has focused on different morphologies, such as nanowires, nanorods, or flower-like structures [36–40]. Notably, flower-like ZnO nanostructures have exhibited superior performance in photocatalysis compared to other shapes, which is attributed to their elevated surface-to-volume ratio [28,41,42]. This feature enables interaction with a greater number of pollutant molecules attached to the surface [43]. Given the primary objective of achieving optimal self-cleaning performance in textiles, this work focuses on investigating flower-like ZnO structures.

To fabricate these structures, our study employs a simple microwave-assisted method. The used technique has shown great potential as an efficient and straightforward route for the growth of ZnO crystals, including the synthesis of textiles [28,44]. The utilization of microwave heating in the process allows a shorter synthesis duration, repeatability, low-cost, and adherence to eco-friendly criteria compared with other methods [25,28,45,46], such as hydrothermal process [15,17,26,40,47]. In addition, current efforts prioritize developing more sustainable methods for synthesizing nanomaterials [25], including reducing the addition of harmful solvents or surfactants, such as cetrimonium bromide (CTAB), which has often been used to achieve desirable crystal shapes [37].

The reaction parameters that can be controlled by this method are, for example, the type of zinc and alkali precursors and their solvent, reaction time, and temperature [29,40,41,47]. As previously reported [41,47], even small changes can have a major impact on the morphology of the final products. The available literature discusses the growth of crystal ZnO structures in different microwave irradiation conditions as well as variable synthesis parameters [48], but there is a lack of a comprehensive analysis of how exactly the synthesis parameters influence the shapes of ZnO crystals. The necessity of understanding this relationship has been highlighted in recent literature [49], particularly the need to identify specific factors contributing to the morphology of ZnO crystals, a gap addressed by our study.

To achieve this objective, we combined diverse protocols from the existing literature into one cohesive experimental framework, providing detailed guidance to empower researchers to readily replicate our results in future experiments. We studied eight parameters from earlier contributions [26,50,51] and combined them into one synthesis protocol to make them directly comparable to each other. Furthermore, our study introduces a self-cleaning test method, employing photo analysis with optimal color representation for quantitative comparisons. This innovative evaluation method, along with the presented aging procedure and protocol suggestions, provides a comprehensive toolkit for exploring the self-cleaning and UV-blocking features of ZnO crystals in textiles.

2. Materials and methods

2.1. Materials

The cotton fabric (140 g/m^2, 100 %) was bought from the Eurokangas store. Details regarding the yarn density include 60 threads/inch for both warp and weft, with a yarn count of 20/1 in both warp and weft. Zinc acetate dehydrate (ZnAc, $(CH_3COO)_2(H_2O)_2$, ≥98 %) and methylene blue (MB, 0.05 wt% in H_2O) was purchased from Sigma-Aldrich. Sodium hydroxide (NaOH, 97 %) and potassium hydroxide (KOH, 88.2 %) were obtained from VWR Chemicals. Ammonium hydroxide (NH_4OH, 50 % v/v) was supplied by Thermo Scientific, and coffee was purchased from a local store. All chemicals were used as provided without further purification. All solutions were prepared with distilled water.

2.2. Pre-treatment of a cotton fabric

To attain a successful ZnO coating, the fabric should be free from any previous chemical finishes. The cotton was cut into squares of 5 cm × 5 cm. To assess the primary color characteristics of the fabric, the whiteness and brightness indices of the untreated cotton sample were determined. This analysis was conducted using the Spectrometer Advantes AvaSpec HS-TEC, equipped with an Ocean Optics LS-1-Cal light source, an integration time of 100.00 ms, and an averaging of 10 spectra per measurement. MgO powder served as the white reference [52,53]. The resulting values were 94.47 for whiteness and 78.90 for brightness, respectively. Color coordinates were further evaluated using the Konica Minolta CM-2300d with firmware version 3.16 [53]. The obtained values were as follows: L* = 85.49, a* = 0.85, b* = 12.32.

The pre-treatment process was started by cleaning the cotton fabrics in a solution of 10 ml of non-ionic detergent Decon90 and 90 ml water, stirred at 60 °C for 15 min to remove any adsorbed impurities from the surface. The fabrics were dried in an oven (Binder, model ED 56) at 50 °C for 12 h. Right before the coating process, the fabrics were kept in 50 ml of 0.1 M sodium hydroxide solution for 10 min to remove impurities, such as fat and proteins [54]. NaOH has also been reported to enhance the surface activity of fibers to improve nanoparticle adhesion when compared with untreated fabrics [55,56].

2.3. Preparation of zinc acetate and synthesis of ZnO nanoflowers

Zinc oxide nanoparticles (ZnO NPs) were fabricated using a modified synthesis process from the literature [26,50,51]. In the process, zinc acetate hydrate (ZnAc later) was dissolved in water at 60 °C for 10 min with vigorous stirring. Next, NH_4OH was added to the mixture dropwise, followed by NaOH or KOH solutions, which resulted in the mixture becoming hazy. The total volume of the reaction was set to 100 ml. The pH of the solution was measured to be approximately 11 using a pH meter (Merck). After combining this mixture, the cotton fabric (5 × 5 cm) was added in a holder to allow continuous stirring during the 6-h seeding process at the set temperature. This step was particularly important in enhancing the adhesion of the ZnO seed layer to the fabric structure. The vessel was transferred into a microwave oven (Asea Scandia, Cylinda EuroLine 170 M) with 800 W power at selected times (3, 4, or 5 min). After the synthesis, samples were washed with deionized water to remove unattached crystals from the textiles' surface and left to dry out in the oven at 50 °C for 12 h.

As an example (Fig. 1), 33 ml of aqueous 0.2 M zinc acetate solution was stirred for 10 min, after which 66 ml of 0.1 M NaOH (aq) and 2 ml of NH_4OH were added to the zinc acetate solution. The textile material was added to the reaction mixture and seeded for 6 h in constant stirring at 300 rpm. After 6 h, the vessel was transferred to a microwave oven and heated for 4 min with 800 W power. The samples were thoroughly washed with deionized water, placed in the oven at 50 °C for 12 h, and dried as described above.

The parameters studied for fabricating flower-like ZnO particles were the concentrations of NaOH, KOH, ZnAc, and NH_4OH, the temperatures of the seeding phase, and the microwave heating time. Detailed experimental protocols can be found in *Table S1* in the Supporting Information section, together with the samples' coding. The repeatability of the methods was confirmed by repeating the experiment protocol a minimum of three times.

2.4. Characterization of ZnO-treated cotton fabric

The crystal structures of the as-prepared samples were examined by XRD using a Pan Analytica diffractometer with $CuK_{\alpha 1}$ radiation (λ = 1.5406 Å) in the 2θ range from 5° to 80° with a tube voltage 45 kV, tube current 40 mA, step size 0.0065 (°), and scanning speed of 0.161 (°)/min. The surface morphologies were studied by Thermo Scientific Apreo S field emission scanning electron microscopy (FE-SEM) operated

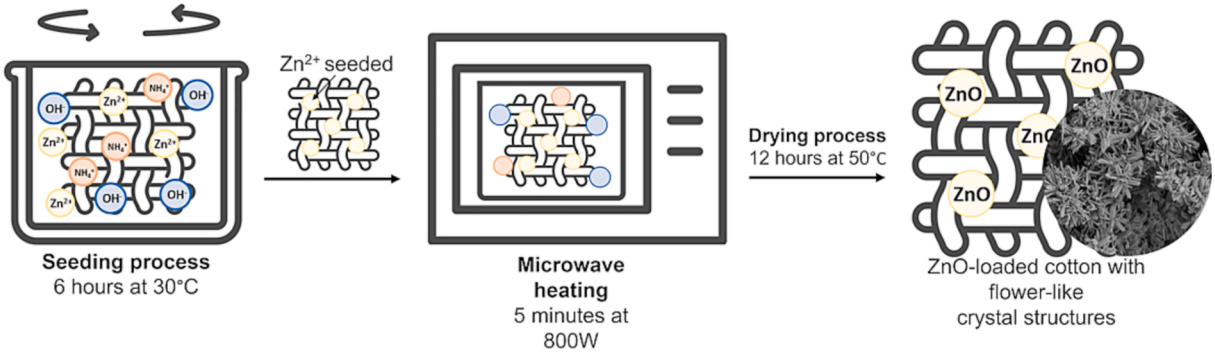

Fig. 1. Schema of a successful process of fabricating ZnO nanoflowers onto a textile substrate.

at HV = 2 kV and current 25 pA. The specimens for SEM analysis were attached to a copper tape and prepared by coating small pieces of each sample with a thin layer of Pt using a plasma coater (Quorum Q150V ES Plus).

To measure both the absorbance and the transmittance of the ZnO-treated cotton, the samples were tested with a UV–Vis Specord 200 Plus spectrophotometer at an absorption wavelength of 200–700 nm, with a measurement step of 1 nm and a scanning speed of 10 nm/s. The UV profiles of the untreated samples were compared with the spectra collected from fabrics treated with ZnO NPs. Measurements were conducted before and after testing the self-cleaning performance. Further, the transmittance data obtained were used to calculate the UPF value.

2.5. Ultraviolet protection factor tests

The protection of uncoated and ZnO-loaded cotton fabrics against UV was investigated using UPF calculations. This is a standardized method published as AS/NZS 4399:1996 and EN 13758–1:2001, and it is widely used to determine the effectiveness of a tested fabric in protecting the skin against UV light [57,58]. The UPF value (Eq. (1) is defined as the ratio of the average effective UV radiance (UVR) (i.e., in the range of 290 to 400 nm) calculated for unprotected skin to the average effective UVR calculated for the skin protected by the fabric, and it is presented as follows:

$$UPF = \frac{\sum_{\lambda=290nm}^{\lambda=400nm} E(\lambda) \times S(\lambda) \times \Delta\lambda}{\sum_{\lambda=290nm}^{\lambda=400nm} E(\lambda) \times S(\lambda) \times T(\lambda) \times \Delta\lambda} \quad (1)$$

where $E(\lambda)$ represents the erythema action spectrum, which shows the relationship between the skin's sensitivity and different wavelengths of ultraviolet radiation in terms of causing sunburn. $S(\lambda)$ is the solar spectral irradiance ($Wm^{-2}nm^{-1}$), $T(\lambda)$ is the spectral transmittance of the fabric at wavelength λ, and $\Delta\lambda$ is the wavelength (nm) interval of the measurements (5 nm in the current work). Values of $E(\lambda)$ and $S(\lambda)$ were taken from a previous study [57].

According to the UPF classification system [57], textiles with UPF values greater than 15 are marked as UV-blocking materials, while textiles with UPF values higher than 40 are categorized as materials with "excellent protection" (Table 1).

The percentage blocking for UV-A (315–400 nm) and UV-B (280–315 nm) was calculated using Eq. (2) and Eq. (3), respectively:

$$100 - \frac{\sum_{\lambda=315\ nm}^{\lambda=400\ nm} T(\lambda) \times \Delta\lambda}{\sum_{\lambda=315\ nm}^{\lambda=400\ nm} \Delta\lambda}\ (\%) \quad (2)$$

$$100 - \frac{\sum_{\lambda=280\ nm}^{\lambda=315\ nm} T(\lambda) \times \Delta\lambda}{\sum_{\lambda=280\ nm}^{\lambda=315\ nm} \Delta\lambda}\ (\%) \quad (3)$$

Table 1
UPF classification system. Standard AS/NZS 4399:1996.

UPF range	UVR protection category	Effective UVR transmission, %
15 to 24	good protection	6.7 to 4.2
25 to 39	very good protection	4.1 to 2.6
40 to 50, 50+	excellent protection	≤ 2.5

2.6. Self-cleaning performance and stability tests

To study the self-cleaning properties, both the ZnO-treated cotton fabrics and uncoated reference samples were exposed to artificial sunlight in an Atlas XLS + solar simulator chamber equipped with a xenon lamp (model NXE 1700). The xenon lamp produced light exposure corresponding to the AM1.5G spectrum (both in the UV and visible range) [59] for a duration of 48 h, with a total radiant exposure in the 300–400 nm wavelength range of approximately 11000 kJ/m^2. The ambient chamber conditions were approximately 36 °C and approximately 10 % relative humidity. To perform the self-cleaning tests, 10 µl droplets of both coffee and MB solutions were applied to the surfaces of the ZnO-coated samples and uncoated references. The coffee was made using a standard drip coffee machine, and 0.005 g of MB was mixed with 100 ml of deionized water.

To monitor visual changes at specific intervals, the samples were taken out of the solar simulator unit and placed in a dedicated photo chamber for photography using a Sony A7 MK2 camera with a Laowa 100 mm f/2.8 macro 2 × lens. The camera settings, including an f/11 aperture, ISO 200 sensitivity, and a shutter speed of 1/20 s, were utilized consistently across the experiment. The chamber was designed with gray-painted walls and illuminated with a uniform light source, an LED strip (LED Neon Flex N-6 × 12-z-11 W-40 k-01, 4000 K color temperature, and a luminous flux of 1150 lm). To ensure accurate color representation in all images, an X-Rite ColorChecker Passport was utilized at the beginning of each photo session. The images were imported into Adobe Photoshop Lightroom Classic (version 12.3) for meticulous white balance and color profile adjustments. This was done to ensure that the observed color changes genuinely reflected the self-cleaning effects and were not confounded by imaging artifacts or potential fading due to textile degradation. Following this, the pictures were saved in JPEG format using 100 % quality settings and Adobe RGB color space. The self-cleaning efficiency of the ZnO-coated fabrics was evaluated using Python script [60] to determine the average RGB values across three distinct areas for both stain types (coffee and MB) on each sample. These areas provide an average color value aimed at closely presenting the true stain color. The uncoated samples served as a baseline, allowing differentiation between color changes attributed to the self-cleaning properties and those caused by degradation due to the accelerated aging test inherent in the cotton fabric itself.

The method of self-cleaning performance analysis is presented in a flowchart (Fig. 2). The aim of this procedure is to highlight the minimum key factors required for quantitative and repeatable analyses.

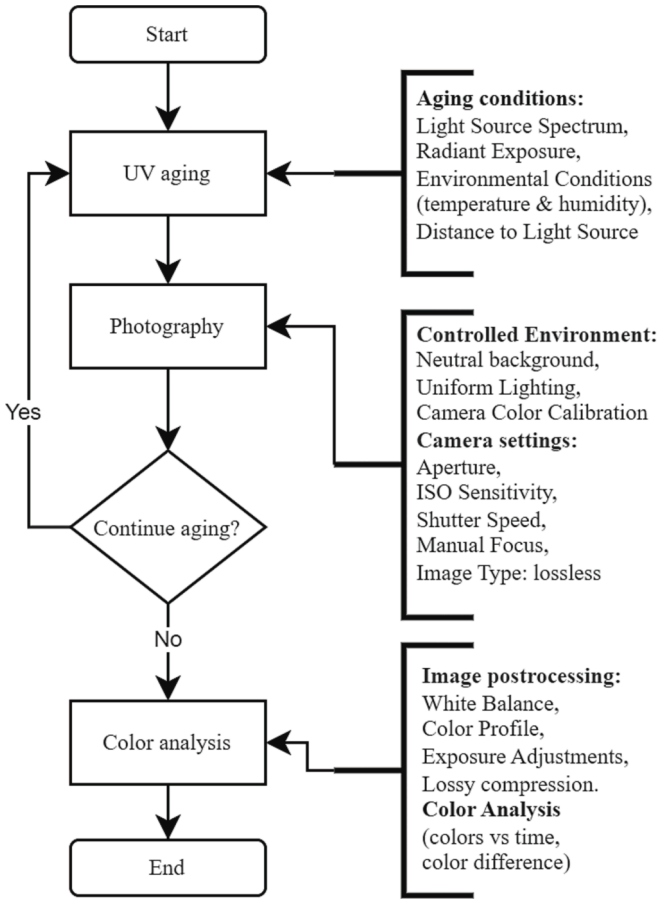

Fig. 2. Flowchart of the methodology for assessing the self-cleaning performance and stability of ZnO-coated fabrics, intended to guide reproducibility in color-tracking investigations.

3. Results and discussion

3.1. Crystalline structure, XRD, and SEM analysis

The outcome of the ZnO growth process on the cotton fabric was studied with XRD measurements, which examined the crystal structures obtained during the synthesis, and SEM, which detected morphological differences in the crystals. XRD patterns are shown in Fig. 3**A**, Fig. 4**A,** and **Fig. S1–S6.** The characteristic reflections of a cellulose structure in the cotton fabric were present at 14.8°, 16.5°, and 22.7° for all samples, as expected [61]. The XRD reflections at 31.74°, 34.38°, 36.22°, 47.54°, °56.58°, and 62.82° indicate the successful growth of the single-phase and crystalline structures of ZnO NPs on the treated cotton fabric. These peaks correspond to the (100), (002), (101), (102), (110), (103), and (112) crystal planes of ZnO, which match the hexagonal wurtzite structure pattern (JCPDS card No. 36–1451) [5,25].

The spectra of samples that used 0.1 and 0.3 M NaOH with NH_4OH solution (samples *0.1NaOH_30°C and 0.3NaOH_30°C*) displayed no additional impurity peaks beyond the expected ZnO signals **(**Fig. 3**A).** This outcome demonstrates that the presented parameters yielded high-purity ZnO. Only in the case of sample *0.2NaOH_30°C* with 0.2 M NaOH solution were $Zn(OH)_2$ XRD patterns noticeable **(**Fig. 3**A).** Furthermore, reducing the concentration of NaOH to 0.1 M induced the desired transition from flake-like structures to flower-like crystals **(**Fig. 3**B).** A closer look at these flower-like crystals showed that they were composed of needle-like and sword-like crystals with an average diameter in the range of 500 nm and 1 μm. Interestingly, increasing the temperature of the stirring process **(Fig. S1)** to 50 °C adversely affected the formation of ZnO; thus, the temperature of further experiments was kept at 30 °C. Since sample *0.1NaOH_30°C* gave the most flower-like shapes, the synthesis procedure was further investigated and improved using these parameters.

To ensure the excess of OH^- and NH_4^+ ions in the reaction [26], the effect of changing the volume of NH_4OH was examined **(Fig. S2).** According to Afzal et al. [51], even small amounts of NH_4OH additive should improve flower-like crystal formation. In both volumes (1 and 2 ml), the XRD patterns revealed that ZnO crystals were obtained in all the syntheses **(Fig. S2A)**, but the difference in morphology was significant **(Fig. S2B).** The addition of 1 ml of NH_4OH resulted in uneven rod-like crystals, and it could even be concluded that some crystals were empty inside, resulting in microtube structures. The introduction of 2 ml of NH_4OH to the solution caused a change in the crystal shapes, creating flower-like structures, as presented earlier (sample *0.1NaOH_30°C)*. We also tested the influence of modifying the ratio between the volumes of NaOH and ZnAc solutions **(Fig. S3).** XRD of the sample *NZ_Ratio11* with a ratio of 1:1 of NaOH and ZnAc exhibited weak peaks of ZnO patterns, while a ratio of 2:1 gave strong signal intensities **(Fig. S3A).** Moreover, we observed that in *NZ_Ratio11*, ZnO crystals formed into uneven bihexagonal rod-like shapes, and a strong aggregation between these

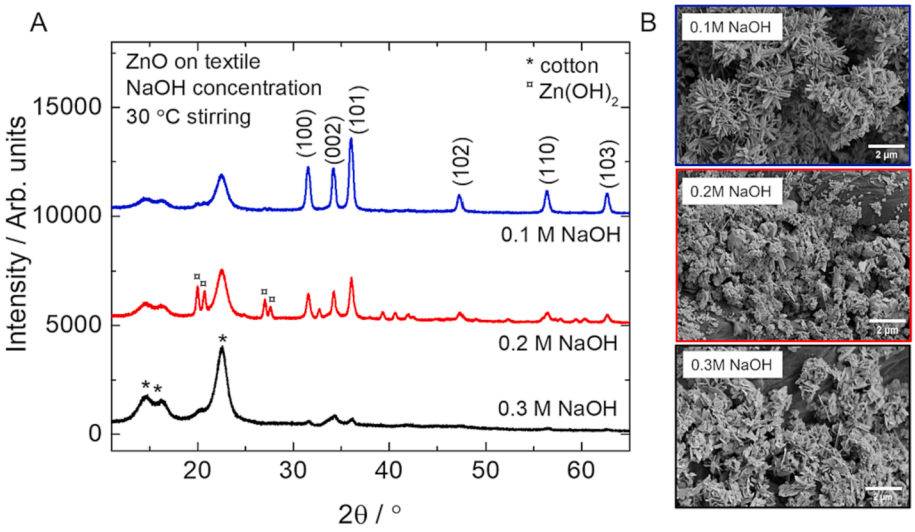

Fig. 3. Patterns of ZnO and $Zn(OH)_2$ crystals formed on cotton substrates using NaOH as a precipitating agent. XRD results **(A)** and corresponding SEM images of the crystal structures **(B)**.

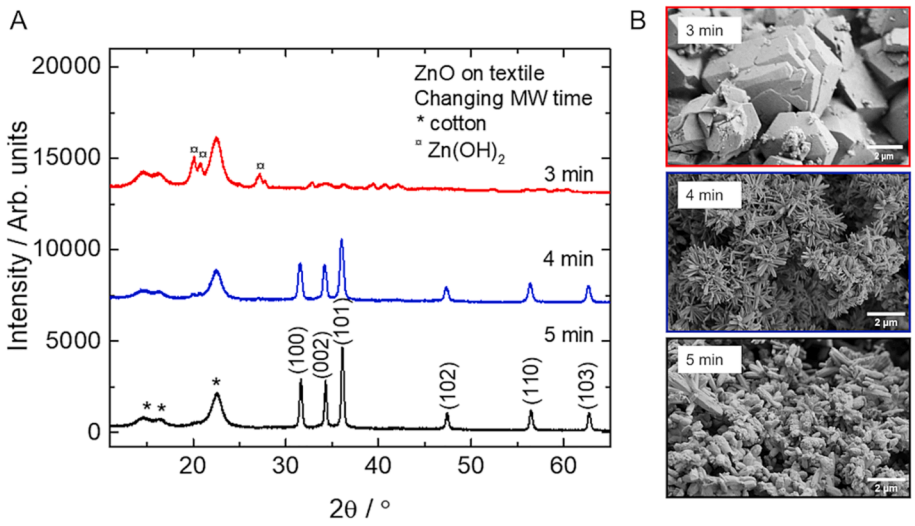

Fig. 4. XRD patterns of ZnO and $Zn(OH)_2$ crystals fabricated on cotton substrates using different microwaving times **(A)** and corresponding SEM images **(B)**.

particles appeared (**Fig. S3B**). These findings indicate that the presence of increased OH^- during synthesis and a higher volume of NH_4OH led to the development of flower-like structures rather than rod-like features.

Further, changing the synthesis time of microwave irradiation showed a significant correlation between the process duration and more intense XRD signals (Fig. 4**A**). Extending the total reaction time from 3 min to 4 min or 5 min caused an improvement in the ZnO formation, which was confirmed with XRD patterns. The presence of residual Zn $(OH)_2$ impurities in the 3-min sample indicates that the energy derived from microwave irradiation was not sufficient to form ZnO nanostructures from $Zn(OH)_2$. The XRD patterns with a longer reaction time were stronger, which could be interpreted as better crystallinity of the ZnO nanostructures on the cotton substrate. This correlation was confirmed by SEM measurements (Fig. 4**B**), in which the sample subjected to a total of 3 min of microwave irradiation (*0.1NaOH_t3*) exhibited bulky-sized $Zn(OH)_2$ crystals, accompanied by the presence of ZnO NPs. Increasing the microwave heating time changed the observed morphology of the materials, suggesting that a smaller ZnO was formed from the decomposition of larger $Zn(OH)_2$ particles. Moreover, the sample *0.1NaOH_30°C* (4 min in total) exhibited substantial aggregation, while the sample *0.1NaOH_t5* (5 min in total irradiation time) achieved exceptional surface coverage, causing the desired broad distribution of particles. Due to these characteristics, the 5-min time parameter was selected for further experiments.

To test another precipitating agent type, 0.1 M, 0.2 M, and 0.3 M KOH solutions were used in the synthesis. XRD signals of crystals obtained through the process showed an analogous pattern to XRD results obtained from samples in which 0.1 M, 0.2 M, and 0.3 M NaOH solutions were used (**Fig. S4A**). The spectra exhibited by samples *0.1KOH_30°C* and *0.3KOH_30°C* showed pure ZnO signals, whereas *0.2KOH_30°C* exhibited peaks indicating $Zn(OH)_2$ appearance. Moreover, the shapes of the crystals varied significantly depending on the concentration of OH^- ions in the primary solution. The SEM images captured the following forms: nanorods, bulky uneven crystals, structures predominantly composed of $Zn(OH)_2$ with minimal presence of ZnO, and nanoflakes (**Fig. S4B**). Since the structures of the obtained crystals did not result in the desired morphology, KOH was excluded from further experiments.

In addition, a varied amount of Zn^{2+} was tested in the synthesis (**Fig. S5**). The XRD measurements showed patterns corresponding to Zn $(OH)_2$ in the cases of both 0.05 M ZnAc and 0.1 M ZnAc parameters, and pure ZnO was obtained only after reaching 0.2 M ZnAc (**Fig. S5A**). This result suggests that the excess of OH^- with the lack of sufficient Zn^{2+} hindered the growth of the desired ZnO structures. In the case of 0.3 M ZnAc, less organized crystal structures, ranging from needle-like to flake-like forms, were recognized (**Fig. S5B**). Moreover, we assessed the effects of changing the ZnAc solvent from H_2O alone to 1:1 H_2O:EtOH or EtOH alone to assess how ZnO growth was affected (**Fig. S6**). Since all three samples exhibited similar signal intensities corresponding to the presence of ZnO, no significant differences were observed (**Fig. S6A**). The SEM images (**Fig. S6B**) captured needle-like and sword-like crystal shapes with bulkier to thinner forms. Thus, H_2O alone, 1:1 H_2O:EtOH and EtOH alone as solvents facilitated the formation of the desired flowerlike structures. In addition, EtOH had more rodlike growth, potentially enhancing coverage on the cotton surface. This characteristic is anticipated to significantly enhance the self-cleaning performance of the material.

It is noteworthy that serious particle aggregation occurred in most of the samples, leading to reduced nanoparticle distribution in certain areas of the surface. This uneven coating coverage can influence self-cleaning and UV-blocking performance. Similarly, the reactivity in photocatalysis is affected by particle sizes; for example, by decreasing the size of ZnO aggregates, hydroxyl radical formation increases [62]. This aggregation is a consequence of the Van der Waals force and the sizes of the crystals, as smaller crystals, due to their nature, are more likely to aggregate [40]. We observed aggregation in samples *0.1NaOH_30°C, 0.1NaOH_N1, NZ_Ratio11, 0.1KOH_30°C,* and *0.3KOH_30°C*, in which smaller particles appeared on the cotton surface and created colonies (Fig. 3**B**, **S2B**, **S3B**, **S4B**). Given the difficulty of breaking down the formed agglomerates [29], it was plausible to proceed with parameters that led to the formation of ZnO coatings with fewer particle agglomerations.

3.2. Possible growth mechanism of ZnO

In our synthesis, we anticipated that the growth mechanism of ZnO would be affected by both the excess of OH^- and the presence of ammonia ions in the reaction mixture. As described in detail in the literature, the presence of hydroxide ions drives the formation of Zn $(OH)_2$ from zinc acetate in the reaction [25,40]. The excess of OH^- in our reaction mixture further drove the formation of the tetrahydrozincate $[Zn(OH)_4]^{2-}$ intermediate complex. In addition to tetrahydrozincate, we also expected that tetraamine zincate $[Zn(NH_3)_4(H2O)_2]^{2+}$ was present in our synthesis due to ammonia used but in smaller quantities. During the microwaving process, both intermediate complexes promoted the formation of ZnO NPs in the synthesis.

The differences in the morphologies of our particles are ascribed to the different ratios of these two intermediate complexes in the synthesis

mixture. The ligands in the tetrahedral $[Zn(OH)_4]^2$ and octahedral $[Zn(NH_3)_4(H2O)_2]^{2+}$ geometries were expected to dissociate at different speeds (Fig. 5**A**). Whereas the sp^3 hybridized OH^- ligands in the tetrahedral complex were assumed to have similar dissociating rates for all the ligands, and the ammonium ligands in the octahedral complex were attached more strongly to the central zinc ion than their water counterparts. This could drive the formation of NPs through the easier detachment of the water ligands, because we only observed spiky-starlike flower structures when we had ammonia present in large quantities in our reaction (Fig. 5**B**). When the amount of ammonia in the synthesis was decreased, a more rodlike structure was present, and a larger amount of NaOH/KOH drove the morphology toward more flake-like structures.

3.3. UV–VIS analysis and ultraviolet protection factor (UPF) values

The UPF values and UV-blocking properties of the coated fabrics were studied with UV–Vis spectroscopy measurements and calculated using Eqs. (1)–(3), respectively. The UVR measurements and spectral data from the Zn-coated samples are presented in Fig. 6**A** and **S7-13**)**A**. To evaluate the stability of the coatings, UV–Vis measurements were taken before (Fig. 6**C**, **S7-13C**) and after the self-cleaning performance tests (Fig. 6**B, D**, **S7-13B, D**) and further compared.

The ZnO particles absorbed UV radiation due to their 3.37 eV bandgap, as reported in the literature [25,63]; however, the fabrics were also good at blocking UV radiation (Fig. 6**A, C,** Table 2**).** The transmission spectra of the plain textile showed that cotton material itself blocked around 98.5 % of both UV radiation and visible light, resulting in a high UV protection (UPF = 80.76 > 50). This outcome likely arose from the pale shade of the yarn and its densely intertwined structure. Therefore, the deposition of ZnO onto textiles characterized by a lower UPF, such as viscose (UPF = 3.0 < 15) [64], is anticipated to confer even greater advantages to the fabric. In all the ZnO-coated materials, the transmission spectra showed values lower than those of the uncoated textile samples, especially in the UV region, exhibiting a value of nearly 100 % in the case of samples with confirmed flower-like structures (Fig. 6**A,** **S7-13A,** Table 2**,** **S2**), confirming their excellent UV-blocking properties. Similar values, approximately 99 %, were given in the visible light spectrum (Fig. 6**A**, **S(7–13)A)**. However, the observed differences between ZnO-coated samples were minimal to such an extent that it was challenging to determine whether these variations arose from the quantity of ZnO present on the surface or were simply a result of inherent fluctuations within the sample and the measurement process. In the absorption spectra displayed in Fig. 6**C** and **Fig. S7-13C**, similar differences can be observed, as the baseline is expected to be the most affected by the varying textile sample. Nonetheless, in all materials, there is higher absorption in the UV range, indicating the presence of ZnO, in addition to the properties of the plain textile that is used as a reference. Subsequently, these values were compared with the UV–Vis measurements obtained from the same samples following a 48-h UV exposure. The differences in transmission data after the aging tests were observed in certain samples (**Fig. S7B, S8B, S13B).** These variations were approximately 1 % and, thus, could be deemed minor when considering the textile-based substrate of the specimens. Moreover, as previously mentioned, these changes could come from natural variations in the samples and the measurement process.

The UPF values for plain and ZnO-coated samples were greater than 50, thus categorizing them as "excellent protection," which is in line with previous studies [26]. However, to judge the improvement of the fabric after applying the ZnO coating, the value differences should be considered. The UPF of samples *0.1NaOH_t5, EtOH_Z*, and *0.3KOH_30°C* were higher than 800, confirming their remarkable protection features (Table 2**,** **S2**). In particular, the sample *EtOH_Z* (i.e., UPF = 1039; UV-A = 99.91; UV-B = 99.94) exhibits excellent performance as a UV blocker (**Table S2**), which is likely attributed to high crystal surface coverage. Moreover, the obtained UV-A and UV-B blocking results are consistent with those in previous studies [26] and better (UV-A and UV-B approximately 99 %) when compared with ZnO coatings made with arginine as a surfactant (UV-A approximately 80 %, UV- B 60–90 %) [25].

3.4. Self-cleaning performance: Photocatalytic degradation of methylene blue and coffee

To assess the self-cleaning performance of ZnO-treated cotton fabrics with different crystal structures and morphologies, samples were stained

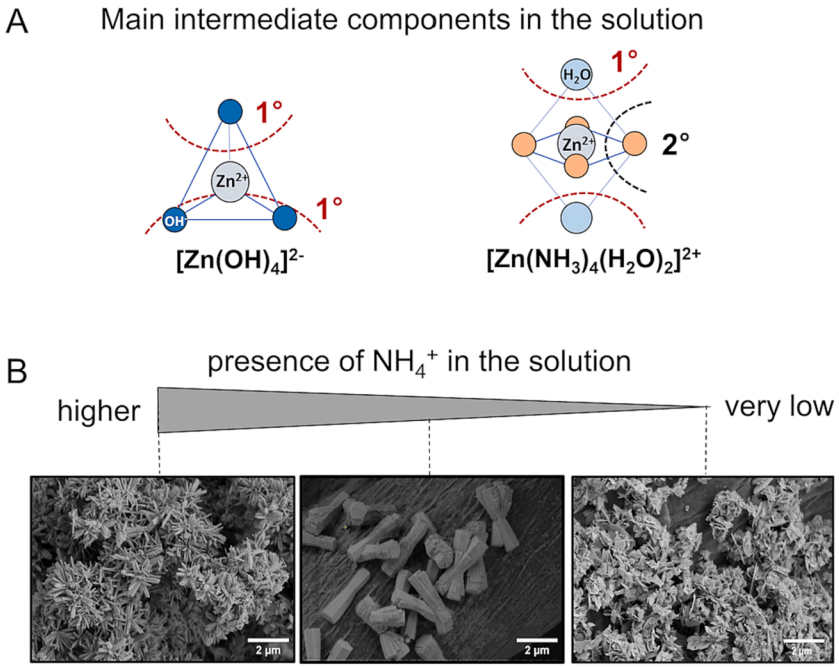

Fig. 5. Schematic illustration of the main intermediate components, represented by a schema of complex geometries **(A)** and the possible outcomes of ZnO crystal growth, as captured by SEM, according to the different amount of NH_4^+ in the solution **(B)**.

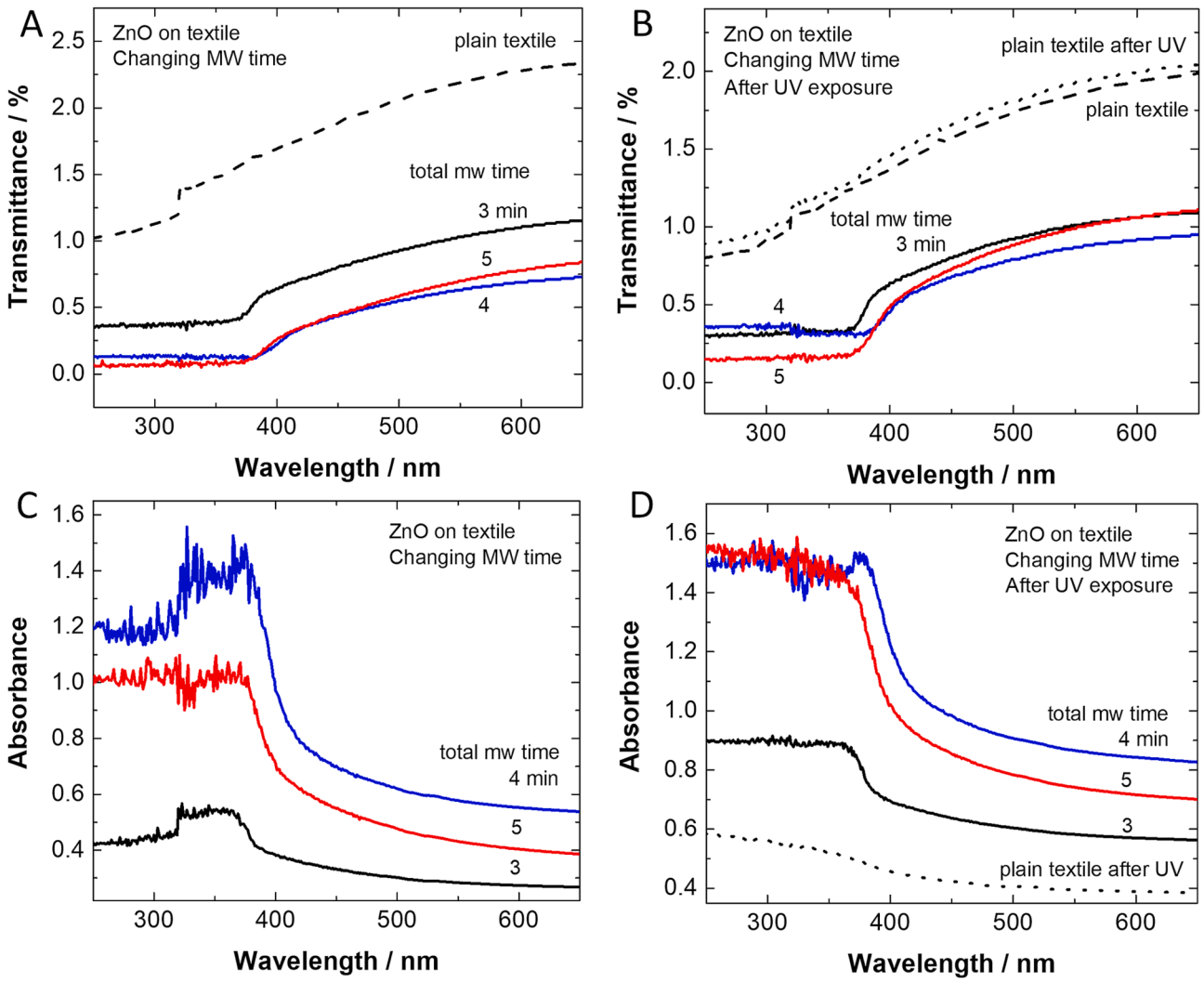

Fig. 6. Transmittance and absorbance measurements of ZnO-coated cotton samples obtained using different microwaving times during the process, before **(A,C)** and after **(B,D)** aging tests.

Table 2
UPF and the UV-A and UV-B blocking efficiency for the examined ZnO-coated samples, obtained using different microwaving times, and their UPF classification.

Sample code	UPF value	UV-blocking efficiency (%)		UPF classification
		UV-A	UV-B	
Reference sample	81	98.49	98.83	excellent protection
0.1NaOH_t3	190	99.55	99.63	excellent protection
0.1NaOH_30°C	589	99.84	99.86	excellent protection
0.1NaOH_t5	883	99.89	99.93	excellent protection

and then exposed to artificial sunlight in a solar simulator chamber for 48 h (Table 3, **S3-S9 Figs. S14, S15**). Samples with strong peaks in Zn $(OH)_2$ XRD patterns were excluded from the self-cleaning evaluation, since $Zn(OH)_2$ lacks photocatalytic properties [65] and presents bulky crystal morphologies with low coverage of the surface area. The tested samples included an uncoated cotton fabric used as a reference. Samples *0.1NaOH_30°C* and *0.1NaOH_t5* were chosen due to their flower-like morphology, which was expected to have good self-cleaning performance [47]. *EtOH_Z* and *0.3NaOH_50°C* were chosen based on their greater photocatalytic efficiency when compared with the other samples. Data from additional samples can be found in the *Supporting Information* (**Tables S3-S4**).

Visually, across all samples, regardless of their initial color, a gradual convergence toward lighter shades was observed over time. This trend is indicative of the aging of cotton substrates under UV exposure. Notably, due to variations in the surface energies among the coatings, differential interactions between droplets and the fabric led to variations in the initial color intensities of the stains. In all samples, MB and coffee stains faded significantly after 5 h of UV exposure, demonstrating effective self-cleaning performance. However, both the rate of degradation of the substrate and the self-cleaning efficiency varied among the samples.

To quantitatively evaluate these changes, the RGB values of the coating surface (later referred to as background), as well as those of the MB and coffee stains, were analyzed separately. By calculating the Euclidean distance [66] of these RGB values at different time points, we determined the percentage variation to represent the color deviation between the chosen points (Table 3, **S4, S7**). The background color changes primarily reflect the fabric's ability to withstand UV light. In all samples, the colors became lighter, indicating UV-driven degradation. However, the extent of this color difference varied among the samples, suggesting variances in their UV resistance (**Table S5**). Specifically, sample *EtOH_Z* maintained the slowest background color change, indicated by a variation of 1.45 % between its initial and final state after 48 h of light exposure (**Table S5**), thus confirming UV blocking. By contrast, the uncoated reference sample underwent a change of

Table 3
Time-series comparison of cotton samples (*Blank, 0.1NaOH_30°C, 0.1NaOH_t5, EtOH_Z, 0.3NaOH_50°C*) showing the discoloration of dyes on cotton at intervals of 0 h, 1 h, 5 h, and 24 h under 1 Sun. Each corresponding photograph showcases a brownish coffee stain in the top left corner (an orange oval on the first image) and a blue MB stain in the bottom right corner (a blue oval), visually depicting the self-cleaning process of the samples. The table also provides two columns for MB and coffee stains, which contain RGB plots as a function of time (up to 5 h).

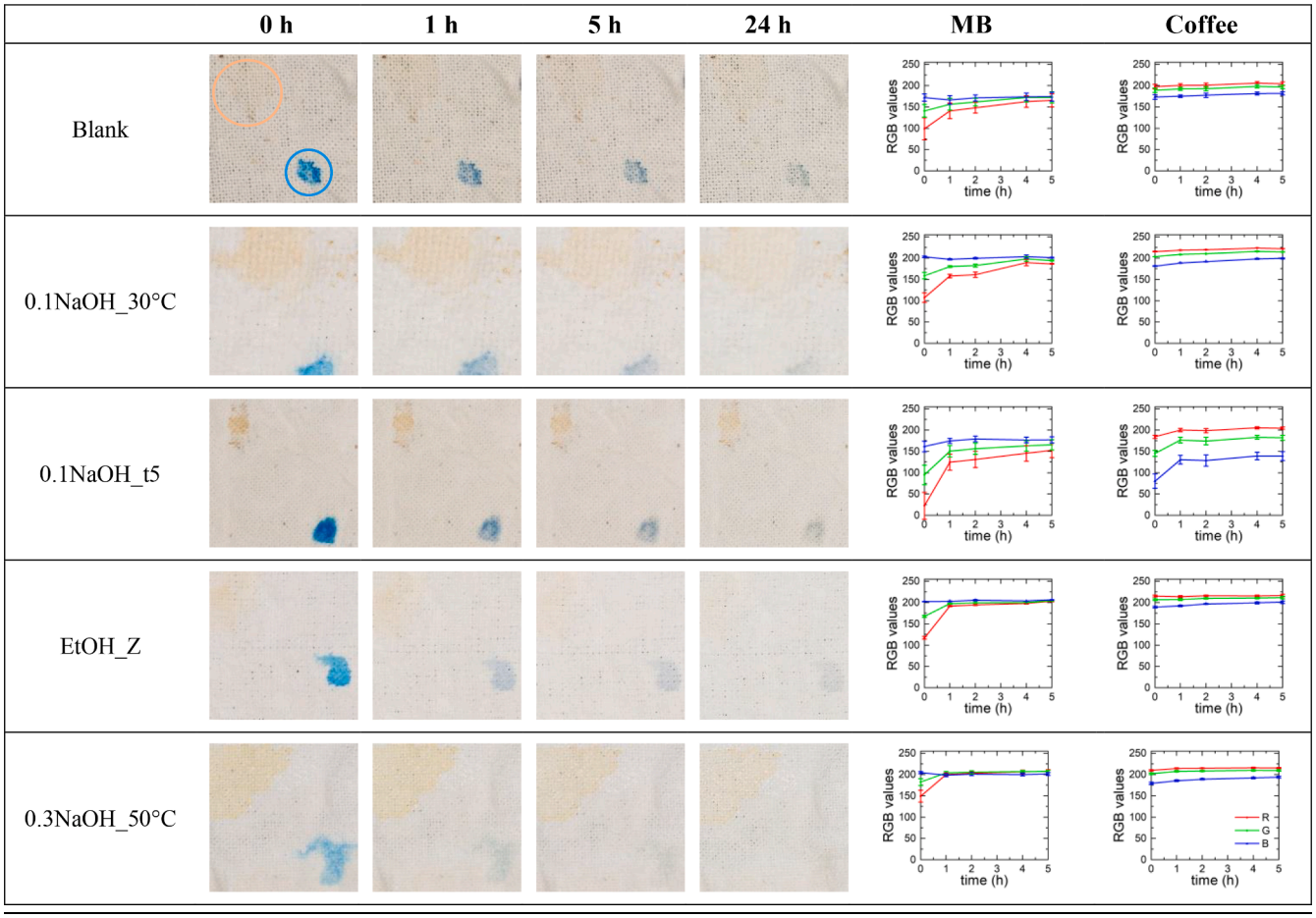

approximately 6 %, implying lower UV resistance.

The MB stains provided insights into the self-cleaning properties of the samples [25]. MB, being UV-degradable [67], showed a color reduction in all samples over time, including in the non-coated reference sample. Therefore, within the first hour, the color of the MB-stained area on a reference sample demonstrated 33 % discoloration efficiency (Table 3, **S8**, **Fig. S14**), and after 24 h, 70 % discoloration efficiency was achieved, proving the photosensitivity of MB. Samples *0.1NaOH_30°C* and *0.1NaOH_t5* displayed color changes of 40 % and 51 %, respectively, after the first hour of light exposure, and 74 % and 77 % after a 24-h period. These outcomes fall below anticipated expectations when compared with the reference, probably due to the low surface coverage of ZnO in both samples. However, samples *0.3NaOH_50°C* and *EtOH_Z* showed remarkable self-cleaning performance (Table 3, **S3, S4, S8**, **Fig. S14**). After just 1 h of 1 sun exposure, the discoloration efficiencies were equal to 72 % and 73 %, respectively. Furthermore, after 24 h, the color of the MB-stained areas of these samples nearly matched their unstained surfaces, with calculated 84 % and 90 % discoloration efficiencies.

Coffee, a widely used drink and a multi-component liquid, provided a realistic alternative for testing the self-cleaning performance of textile-based substrates. Within the first hour of the discoloration process, the coffee stain removal efficiency of the reference sample was 15 % and did not change during the 24-h period (Table 3, **S3, S4, S8, S9**, **Fig. S15**). By contrast, samples *0.1NaOH_30°C* and *0.1NaOH_t5* showed a higher color fade, with 22 % and 53 % efficiencies, respectively. After 24 h, these values increased, reaching 64 % and 60 %, respectively. Samples *0.3NaOH_50°C* and *EtOH_Z* discolored the coffee stains with 23 % and 32 % efficiencies within 1 h of 1 Sun exposure. These values increased by 67 % and 82 % after 24 h of the process, which underlined their self-cleaning performance. These results are remarkable, as in the previous literature, no self-cleaning was observed with such low humidity, as 60 % humidity was required to perform self-cleaning on coffee when visual degradation was studied [26].

Overall, both samples *0.1NaOH_30°C* and *0.1NaOH_t5* with flower-like structures were expected to provide the best self-cleaning performance; however, samples *0.3NaOH_50°C* and *EtOH_Z* showed fast and best fading among our samples. This confirms our previous assumptions that factors beyond the crystal structure of the ZnO coating, such as surface coverage and particle size, are likely to greatly influence the efficiency of the photocatalysis process.

However, although our study used a detailed and systematic approach to evaluate the self-cleaning efficiency of ZnO-coated fabrics, direct comparison with existing research is challenging (**Table S10**), as varied light sources, different stain types, and divergent analytical methods across studies add complexity to any comparison [25,26,68–70]. Additionally, some studies lacked specific data points, such as environmental conditions or quantitative analysis methods, which can complicate one-to-one comparisons. For instance, [70] presented data on the discoloration efficiency of MB values between 1 and 20 % following 24 and 42 h of sunlight exposure. This study compared the color differences between untreated and ZnO NPs-treated fabrics,

with color parameters measured via a reflectance spectrophotometer. However, essential information regarding light intensity, the environmental conditions during the self-cleaning process, and MB concentration was notably absent, impeding comparative analysis. Another example documented in [26], explored the color alteration in both untreated and ZnO NPs treated samples, using milk coffee as the stain source. In this study, the color analysis relied on the visual inspection approach, lacking specification on the image analysis settings and conditions. Therefore, it is not possible to compare that data with our results. The closest comparable study is [25], in which the efficiency of MB degradation reached 30–40 % after 1 h of sun exposure, while our best textiles yielded approximately double this value.

3.5. Mechanism of photocatalysis of ZnO

The photocatalysis-based self-cleaning mechanism relies on decontamination in the presence of solar illumination initiated on the surface of photocatalytic nanomaterials, as explained in [12]. The process is triggered by introducing a light source with energy equivalent to or higher than the band gap of the photocatalyst. This energy is sufficient to transfer electrons from the valence band to the conduction band, forming electron–hole pairs (Fig. 7**A**). There are three possible pathways for photogenerated pairs: (1) a swift recombination of electron–hole pairs either on the surface or within the bulk of photocatalysis; (2) photoreduction, electrons (e^-) interact with oxygen molecules in the air, generating superoxide anion radicals ($\cdot O_2^-$) on the material's surface; and (3) photooxidation, positive holes (h^+) oxidize water molecules present in the humidity of the air and generate highly oxidizing hydroxyl radicals (OH).

Formed radicals are highly chemically reactive and decompose pollutants adhered to the surface of the material, such as dirt or organic contamination, into carbon dioxide and water molecules. ZnO NPs absorb UV light with wavelengths shorter than 380 nm, which is the ZnO band gap [5]. This phenomenon leads to the degradation of methylene blue and coffee stains on the fabric surface in the presence of a light source (Fig. 7**B**).

4. Conclusion

In this work, we fabricated self-cleaning textiles by applying photocatalytic flower-like ZnO nanostructures to cotton substrates. Our study comprehensively documents and evaluates the factors governing the growth of ZnO crystals while concurrently affirming the self-cleaning performance and UV blocking of fabricated ZnO-loaded fabrics. The best protocol to achieve self-cleaning ZnO-coated cotton without using surfactants was found to be a solution of 66 ml of 0.1 M NaOH, 33 ml of 0.2 M ZnAc dissolved in EtOH, and 2 ml of NH_4OH and a microwave treatment for 5 min.

We found that 0.1 M NaOH concentration gave flower-like structures, while crystals grown assisted with (0.1–0.3) M KOH solutions exhibited less favorable structures. Regarding energy consumption, the stirring temperature of 30 °C and the time in the microwave of 5 min was sufficient to obtain the desired crystal structures repeatedly. Overall, 2 ml of NH_4OH was sufficient to achieve a flower-like morphology. Crystal structures made with water as a ZnAc solvent looked more promising, but self-cleaning tests showed that the coating obtained with EtOH performed better. The improved performance of the samples with EtOH was attributed to the increased surface coverage of the ZnO crystals, which was confirmed through SEM characterization.

Our ZnO-coated textiles exhibited excellent UV-blocking characteristics (nearly 100 %), as confirmed by the UPF values. Moreover, in the self-cleaning tests performed with coffee and MB stains, the fastest fading rates of the contaminations were obtained in sample *0.3NaOH_50°C*, fabricated using 0.3 M NaOH at 50 °C with water used as a solvent to achieve flake-like ZnO morphologies, and sample *EtOH_Z*, fabricated using 0.1 M NaOH at 30 °C with ethanol to achieve flower-like ZnO morphologies. The most effective coating (*EtOH_Z*) showed an MB dye degradation of 73 % within the first hour of UV exposure, which increased to 90 % after 24 h. These results seem promising, since they double the efficiency values reported in the most related previous

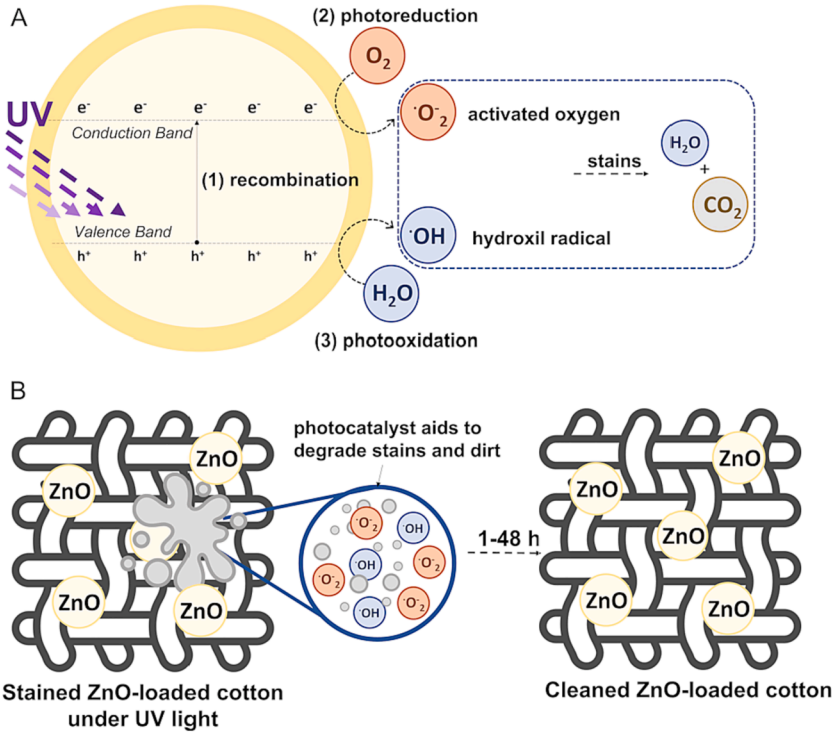

Fig. 7. Schematic illustration of the photocatalytic activity of ZnO under UV light **(A)**. Schema of the self-cleaning process appearing on a Zn-coated textile surface, based on photocatalysis **(B)**.

study. The proficient performance of these samples can be attributed to their greater surface coverage compared to other samples made using our protocol. Hence, the significance of achieving even particle distribution on the surface has to be highlighted to enhance the photocatalysis process.

CRediT authorship contribution statement

Alicja Lawrynowicz: Conceptualization, Methodology, Validation, Formal analysis, Investigation, Writing – original draft, Visualization. **Emilia Palo:** Formal analysis, Writing – review & editing, Visualization, Supervision. **Rustem Nizamov:** Formal analysis, Investigation, Data Curation, Software, Writing – review & editing. **Kati Miettunen:** Writing – review & editing, Supervision, Project administration, Funding acquisition.

Declaration of competing interest

The authors declare that they have no known competing financial interests or personal relationships that could have appeared to influence the work reported in this paper.

Data availability

Data will be made available on request.

Acknowledgments

This work was (partly) supported by NordForsk through the funding to Nordic network on smart light-conversion textiles beyond electric circuits, project number 103894. Special thanks to Mikael Nyberg and the whole team of lab engineers for providing technical help. Thanks to Dr. Heikki Palonen for the XRD introduction and Dr. Sami Vuori for the assistance in conducting spectrometry measurements.

Appendix A. Supplementary data

Supplementary data to this article can be found online at https://doi.org/10.1016/j.jphotochem.2023.115420.

References

[1] T. Suryaprabha, M.G. Sethuraman, A Facile Approach for Fabrication Superhydrophobic and UV-blocking Cotton Fabrics with Self-cleaning Properties, Fibers Polym. 22 (2021) 1033–1040, https://doi.org/10.1007/s12221-021-0648-z.

[2] G. Kibria, M.R. Repon, M.F. Hossain, T. Islam, M.A. Jalil, M.D. Aljabri, M. M. Rahman, UV-blocking cotton fabric design for comfortable summer wears: factors, durability and nanomaterials, Cellulose. 29 (2022) 7555–7585, https://doi.org/10.1007/s10570-022-04710-7.

[3] E. Kobina Sam, D. Kobina Sam, X. Lv, B. Liu, X. Xiao, S. Gong, W. Yu, J. Chen, J. Liu, Recent development in the fabrication of self-healing superhydrophobic surfaces, Chemical Engineering Journal. 373 (2019) 531–546, https://doi.org/10.1016/j.cej.2019.05.077.

[4] S. Schneegass, O. Amft, eds., Smart Textiles: Fundamentals, Design, and Interaction, Springer International Publishing, Cham, 2017. https://doi.org/10.1007/978-3-319-50124-6.

[5] S. Ghayempour, M. Montazer, Ultrasound irradiation based in-situ synthesis of star-like Tragacanth gum/zinc oxide nanoparticles on cotton fabric, Ultrasonics Sonochemistry. 34 (2017) 458–465, https://doi.org/10.1016/j.ultsonch.2016.06.019.

[6] B. Su, Y. Tian, L. Jiang, Bioinspired Interfaces with Superwettability: From Materials to Chemistry, J. Am. Chem. Soc. 138 (2016) 1727–1748, https://doi.org/10.1021/jacs.5b12728.

[7] S. Li, J. Huang, Z. Chen, G. Chen, Y. Lai, A review on special wettability textiles: theoretical models, fabrication technologies and multifunctional applications, J. Mater. Chem. a. 5 (2017) 31–55, https://doi.org/10.1039/C6TA07984A.

[8] T. Fan, R. Hu, Z. Zhao, Y. Liu, M. Lu, Surface micro-dissolve method of imparting self-cleaning property to cotton fabrics in NaOH/urea aqueous solution, Applied Surface Science. 400 (2017) 524–529, https://doi.org/10.1016/j.apsusc.2016.12.184.

[9] J. Wang, J. Zhao, L. Sun, X. Wang, A review on the application of photocatalytic materials on textiles, Textile Research Journal. 85 (2015) 1104–1118, https://doi.org/10.1177/0040517514559583.

[10] X. Zhang, J. Villafuerte, V. Consonni, J.-F. Capsal, P.-J. Cottinet, L. Petit, M.-Q. Le, Characterizing and Optimizing Piezoelectric Response of ZnO Nanowire/PMMA Composite-Based Sensor, Nanomaterials. 11 (2021) 1712, https://doi.org/10.3390/nano11071712.

[11] D. Sahu, G.M. Kannan, R. Vijayaraghavan, Size-Dependent Effect of Zinc Oxide on Toxicity and Inflammatory Potential of Human Monocytes, Journal of Toxicology and Environmental Health, Part A 77 (2014) 177–191, https://doi.org/10.1080/15287394.2013.853224.

[12] E. Pakdel, J. Wang, S. Kashi, L. Sun, X. Wang, Advances in photocatalytic self-cleaning, superhydrophobic and electromagnetic interference shielding textile treatments, Advances in Colloid and Interface Science. 277 (2020), 102116, https://doi.org/10.1016/j.cis.2020.102116.

[13] X.-T. Zhang, O. Sato, M. Taguchi, Y. Einaga, T. Murakami, A. Fujishima, Self-Cleaning Particle Coating with Antireflection Properties, Chem. Mater. 17 (2005) 696–700, https://doi.org/10.1021/cm0484201.

[14] V.V. Shinde, D.S. Dalavi, S.S. Mali, C.K. Hong, J.H. Kim, P.S. Patil, Surfactant free microwave assisted synthesis of ZnO microspheres: Study of their antibacterial activity, Applied Surface Science. 307 (2014) 495–502, https://doi.org/10.1016/j.apsusc.2014.04.064.

[15] M.Z. Khan, V. Baheti, J. Militky, J. Wiener, A. Ali, Self-cleaning properties of polyester fabrics coated with flower-like TiO 2 particles and trimethoxy (octadecyl) silane, Journal of Industrial Textiles. 50 (2020) 543–565, https://doi.org/10.1177/1528083719836938.

[16] F. Fu, L. Li, L. Liu, J. Cai, Y. Zhang, J. Zhou, L. Zhang, Construction of Cellulose Based ZnO Nanocomposite Films with Antibacterial Properties through One-Step Coagulation, ACS Appl. Mater. Interfaces. 7 (2015) 2597–2606, https://doi.org/10.1021/am507639b.

[17] K.U. Rahman, E.P. Ferreira-Neto, G.U. Rahman, R. Parveen, A.S. Monteiro, G. Rahman, Q. Van Le, R.R. Domeneguetti, S.J.L. Ribeiro, S. Ullah, Flexible bacterial cellulose-based BC-SiO2-TiO2-Ag membranes with self-cleaning, photocatalytic, antibacterial and UV-shielding properties as a potential multifunctional material for combating infections and environmental applications, Journal of Environmental Chemical Engineering. 9 (2021), 104708, https://doi.org/10.1016/j.jece.2020.104708.

[18] I.H. Mondal, Antimicrobial Textiles from Natural Resources, Woodhead Publishing (2021), https://doi.org/10.1016/B978-0-12-821485-5.00016-0.

[19] K.S. Siddiqi, A. ur Rahman, Tajuddin, A. Husen, Properties of Zinc Oxide Nanoparticles and Their Activity Against Microbes, Nanoscale Res Lett. 13 (2018) 141, https://doi.org/10.1186/s11671-018-2532-3.

[20] Sadia Afroz, Md. Arif Roman Azady, Yeasmin Akter, Abdullah Al Ragib, Zahid Hasan, Md. Saifur Rahaman, Jahid M M Islam, Self-cleaning textiles: structure, fabrication and applications, in: Md. Ibrahim, H. Mondal (Eds.), Fundamentals of Natural Fibres and Textiles, Elsevier, 2021: pp. 557–597. https://doi.org/10.1016/B978-0-12-821483-1.00030-9.

[21] C. Zhu, A. Mochizuki, J. Shi, M. Ishimori, S. Koyama, H. Ishizawa, J. Yan, H. Morikawa, Photocatalytic self-cleaning coatings to remove oleic acid, an organic pollutant, from cotton fabrics, Cellulose. 28 (2021) 8139–8152, https://doi.org/10.1007/s10570-021-04004-4.

[22] H. Gaminian, M. Montazer, Simultaneous nano TiO2 sensitization, application and stabilization on polyester fabric using madder and NaOH producing enhanced self-cleaning with hydrophilic properties under visible light, Journal of Photochemistry and Photobiology a: Chemistry. 332 (2017) 158–166, https://doi.org/10.1016/j.jphotochem.2016.08.022.

[23] E. Busi, S. Maranghi, L. Corsi, R. Basosi, Environmental sustainability evaluation of innovative self-cleaning textiles, Journal of Cleaner Production. 133 (2016) 439–450, https://doi.org/10.1016/j.jclepro.2016.05.072.

[24] S. Mollick, M.R. Repon, A. Haji, M.A. Jalil, T. Islam, M.M. Khan, Progress in self-cleaning textiles: parameters, mechanism and applications, Cellulose. (2023), https://doi.org/10.1007/s10570-023-05539-4.

[25] M.A. Tănase, A.C. Soare, P. Oancea, A. Răducan, C.I. Mihăescu, E. Alexandrescu, C. Petcu, L.M. Diţu, M. Ferbinteanu, B. Cojocaru, L.O. Cinteza, Facile In Situ Synthesis of ZnO Flower-like Hierarchical Nanostructures by the Microwave Irradiation Method for Multifunctional Textile Coatings, Nanomaterials. 11 (2021) 2574, https://doi.org/10.3390/nano11102574.

[26] V.H. Tran Thi, B.-K. Lee, Development of multifunctional self-cleaning and UV blocking cotton fabric with modification of photoactive ZnO coating via microwave method, Journal of Photochemistry and Photobiology a: Chemistry. 338 (2017) 13–22, https://doi.org/10.1016/j.jphotochem.2017.01.020.

[27] V. Batra, I. Kaur, D. Pathania, Sonu, V, Chaudhary, Efficient Dye Degradation Strategies Using Green Synthesized ZnO-Based Nanoplatforms: A Review, Applied Surface Science Advances. 11 (2022), 100314, https://doi.org/10.1016/j.apsadv.2022.100314.

[28] J. Wojnarowicz, T. Chudoba, W. Lojkowski, A Review of Microwave Synthesis of Zinc Oxide Nanomaterials: Reactants, Process Parameters and Morphologies, Nanomaterials. 10 (2020) 1086, https://doi.org/10.3390/nano10061086.

[29] A. Kołodziejczak-Radzimska, T. Jesionowski, Zinc Oxide—From Synthesis to Application: A Review, Materials. 7 (2014) 2833–2881, https://doi.org/10.3390/ma7042833.

[30] Y. Sun, L. Chen, Y. Bao, Y. Zhang, J. Wang, M. Fu, J. Wu, D. Ye, The Applications of Morphology Controlled ZnO in Catalysis, Catalysts. 6 (2016) 188, https://doi.org/10.3390/catal6120188.

[31] B. Lallo Da Silva, B.L. Caetano, B.G. Chiari-Andréo, R.C.L.R. Pietro, L.A. Chiavacci, Increased antibacterial activity of ZnO nanoparticles: Influence of size and surface modification, Colloids and Surfaces b: Biointerfaces. 177 (2019) 440–447, https://doi.org/10.1016/j.colsurfb.2019.02.013.

[32] K.T. Kim, M.Y. Eo, T.T.H. Nguyen, S.M. Kim, General review of titanium toxicity, Int J Implant Dent. 5 (2019) 10, https://doi.org/10.1186/s40729-019-0162-x.
[33] Y. He, M. Wan, Z. Wang, X. Zhang, Y. Zhao, L. Sun, Fabrication and characterization of degradable and durable fluoride-free super-hydrophobic cotton fabrics for oil/water separation, Surface and Coatings Technology. 378 (2019), 125079, https://doi.org/10.1016/j.surfcoat.2019.125079.
[34] S.S. Alias, A.A. Mohamad, Synthesis of Zinc Oxide by Sol-Gel Method for Photoelectrochemical Cells, Springer Singapore, Singapore (2014), https://doi.org/10.1007/978-981-4560-77-1.
[35] N. Talebian, S.M. Amininezhad, M. Doudi, Controllable synthesis of ZnO nanoparticles and their morphology-dependent antibacterial and optical properties, Journal of Photochemistry and Photobiology b: Biology. 120 (2013) 66–73, https://doi.org/10.1016/j.jphotobiol.2013.01.004.
[36] L. Li, H. Yang, H. Zhao, J. Yu, J. Ma, L. An, X. Wang, Hydrothermal synthesis and gas sensing properties of single-crystalline ultralong ZnO nanowires, Appl. Phys. a. 98 (2010) 635–641, https://doi.org/10.1007/s00339-009-5457-y.
[37] X. Jiaqiang, C. Yuping, C. Daoyong, S. Jianian, Hydrothermal synthesis and gas sensing characters of ZnO nanorods, Sensors and Actuators b: Chemical. 113 (2006) 526–531, https://doi.org/10.1016/j.snb.2005.03.097.
[38] C. Jiang, W. Liu, M. Yang, C. Liu, S. He, Y. Xie, Z. Wang, Facile fabrication of robust fluorine-free self-cleaning cotton textiles with superhydrophobicity, photocatalytic activity, and UV durability, Colloids and Surfaces a: Physicochemical and Engineering Aspects. 559 (2018) 235–242, https://doi.org/10.1016/j.colsurfa.2018.09.048.
[39] C.M. Chang, M.H. Hon, I.C. Leu, Preparation of ZnO nanorod arrays with tailored defect-related characterisitcs and their effect on the ethanol gas sensing performance, Sensors and Actuators b: Chemical. 151 (2010) 15–20, https://doi.org/10.1016/j.snb.2010.09.072.
[40] L. Zhu, Y. Li, W. Zeng, Hydrothermal synthesis of hierarchical flower-like ZnO nanostructure and its enhanced ethanol gas-sensing properties, Applied Surface Science. 427 (2018) 281–287, https://doi.org/10.1016/j.apsusc.2017.08.229.
[41] A. Kajbafvala, H. Ghorbani, A. Paravar, J.P. Samberg, E. Kajbafvala, S. K. Sadrnezhaad, Effects of morphology on photocatalytic performance of Zinc oxide nanostructures synthesized by rapid microwave irradiation methods, Superlattices and Microstructures. 51 (2012) 512–522, https://doi.org/10.1016/j.spmi.2012.01.015.
[42] N. Kaneva, I. Stambolova, V. Blaskov, Y. Dimitriev, A. Bojinova, C. Dushkin, A comparative study on the photocatalytic efficiency of ZnO thin films prepared by spray pyrolysis and sol–gel method, Surface and Coatings Technology. 207 (2012) 5–10, https://doi.org/10.1016/j.surfcoat.2011.10.020.
[43] L. Wang, Y. Kang, X. Liu, S. Zhang, W. Huang, S. Wang, ZnO nanorod gas sensor for ethanol detection, Sensors and Actuators b: Chemical. 162 (2012) 237–243, https://doi.org/10.1016/j.snb.2011.12.073.
[44] D.J. da Silva, R.F. da Silva Barbosa, A.G. de Souza, R.R. Ferreira, P.H. Camani, I. L. Nantes-Cardoso, D.S. Rosa, Bactericidal activity of cotton fabrics functionalized by ZnO and Cu via microwave, Cellulose. 28 (2021) 8153–8175, https://doi.org/10.1007/s10570-021-03990-9.
[45] A. Kajbafvala, S. Zanganeh, E. Kajbafvala, H.R. Zargar, M.R. Bayati, S. K. Sadrnezhaad, Microwave-assisted synthesis of narcis-like zinc oxide nanostructures, Journal of Alloys and Compounds. 497 (2010) 325–329, https://doi.org/10.1016/j.jallcom.2010.03.057.
[46] M.Z. Khan, H. Taghavian, M. Fijalkowski, J. Militky, B. Tomkova, M. Venkataraman, K. Adach, Effect of microwave power on bactericidal and UV protection properties of the ZnO nanorods grown cotton fabrics, Colloids and Surfaces a: Physicochemical and Engineering Aspects. 664 (2023), 131135, https://doi.org/10.1016/j.colsurfa.2023.131135.
[47] X. Zou, J. Ke, J. Hao, X. Yan, Y. Tian, A new method for synthesis of ZnO flower-like nanostructures and their photocatalytic performance, Physica b: Condensed Matter. 624 (2022), 413395, https://doi.org/10.1016/j.physb.2021.413395.
[48] E. Mohammadi, M. Aliofkhazraei, M. Hasanpoor, M. Chipara, Hierarchical and Complex ZnO Nanostructures by Microwave-Assisted Synthesis: Morphologies, Growth Mechanism and Classification, Critical Reviews in Solid State and Materials Sciences. 43 (2018) 475–541, https://doi.org/10.1080/10408436.2017.1397501.
[49] B. Clarke, K. Ghandi, The Interplay of Growth Mechanism and Properties of ZnO Nanostructures for Different Applications, Small. (2023) 2302864, https://doi.org/10.1002/smll.202302864.
[50] D. Raoufi, Synthesis and microstructural properties of ZnO nanoparticles prepared by precipitation method, Renewable Energy. 50 (2013) 932–937, https://doi.org/10.1016/j.renene.2012.08.076.
[51] S. Moungsrijun, S. Sujinnapram, S. Sutthana, Synthesis and characterization of zinc oxide prepared with ammonium hydroxide and photocatalytic application of organic dye under ultraviolet illumination, Monatsh Chem. 148 (2017) 1177–1183, https://doi.org/10.1007/s00706-017-1959-z.
[52] H. Jung, Comparison between the Color Properties of Whiteness Index and Yellowness Index on the CIELAB, Textile Coloration and Finishing. 25 (2013) 241–246, https://doi.org/10.5764/TCF.2013.25.4.241.
[53] A.K. Samanta, P. Agarwal, S. Datta, Dyeing of jute with binary mixtures of jackfruit wood and other natural dyes — Study on colour performance and dye compatibility, INDIAN J. FIBRE TEXT. RES. (2008).
[54] W. Ouarhim, N. Zari, R. Bouhfid, A.E.K. Qaiss, Mechanical performance of natural fibers–based thermosetting composites, in: Mechanical and Physical Testing of Biocomposites, Fibre-Reinforced Composites and Hybrid Composites, Elsevier, 2019, pp. 43–60, https://doi.org/10.1016/B978-0-08-102292-4.00003-5.
[55] S.M.T. Shahin, M. Montazer, Diverse-shaped ZnO nanoparticles on polyester fabric through assorted *in situ* methods: studying plasma treatment order and different alkali media, The Journal of the Textile Institute. 112 (2021) 1788–1803, https://doi.org/10.1080/00405000.2020.1843256.
[56] M.E. Yazdanshenas, M. Shateri-Khalilabad, The effect of alkali pre-treatment on formation and adsorption of silver nanoparticles on cotton surface, Fibers Polym. 13 (2012) 1170–1178, https://doi.org/10.1007/s12221-012-1170-0.
[57] Sun protective clothing, evaluation and classification, Standards Australia; Standards New Zealand, Homebush, NSW, Wellington, N.Z., 1996.
[58] T. Gambichler, J. Laperre, K. Hoffmann, The European standard for sun-protective clothing: EN 13758, J Eur Acad Dermatol Venerol. 20 (2006) 125–130, https://doi.org/10.1111/j.1468-3083.2006.01401.x.
[59] A. Poskela, K. Miettunen, A. Tiihonen, P.D. Lund, Extreme sensitivity of dye solar cells to UV-induced degradation, Energy Science & Engineering. 9 (2020) 9–26, https://doi.org/10.1002/ese3.810.
[60] R. Nizamov, RGB_recognition, (2023). https://gitlab.com/mateng-utu/RGB_recognition.
[61] S. Afzal, W.A. Daoud, S.J. Langford, Visible-light self-cleaning cotton by metalloporphyrin-sensitized photocatalysis, Applied Surface Science. 275 (2013) 36–42, https://doi.org/10.1016/j.apsusc.2013.01.141.
[62] S. Shrestha, B. Wang, P. Dutta, Nanoparticle processing: Understanding and controlling aggregation, Advances in Colloid and Interface Science. 279 (2020), 102162, https://doi.org/10.1016/j.cis.2020.102162.
[63] O.K. Alebeid, T. Zhao, Review on: developing UV protection for cotton fabric, The Journal of the Textile Institute. 108 (2017) 2027–2039, https://doi.org/10.1080/00405000.2017.1311201.
[64] N.S. Heliopoulos, G.N. Kouzilos, A.I. Giarmenitis, S.K. Papageorgiou, K. Stamatakis, F.K. Katsaros, Viscose Fabric Functionalized with Copper and Copper Alginate Treatment Toward Antibacterial and UV Blocking Properties, Fibers Polym. 21 (2020) 1238–1250, https://doi.org/10.1007/s12221-020-9578-4.
[65] Y. Wu, S. Zeng, Y. Dong, Y. Fu, H. Sun, S. Yin, X. Guo, W. Qin, Hydrogen production from methanol aqueous solution by ZnO/Zn(OH) 2 macrostructure photocatalysts, RSC Adv. 8 (2018) 11395–11402, https://doi.org/10.1039/C8RA00943K.
[66] M.T. Noman, J. Militky, J. Wiener, J. Saskova, M.A. Ashraf, H. Jamshaid, M. Azeem, Sonochemical synthesis of highly crystalline photocatalyst for industrial applications, Ultrasonics. 83 (2018) 203–213, https://doi.org/10.1016/j.ultras.2017.06.012.
[67] M.G. Kim, J.E. Lee, K.S. Kim, J.M. Kang, J.H. Lee, K.H. Kim, M. Cho, S.G. Lee, Photocatalytic degradation of methylene blue under UV and visible light by brookite–rutile bi-crystalline phase of TiO $_2$, New J. Chem. 45 (2021) 3485–3497, https://doi.org/10.1039/D0NJ05162D.
[68] M. Ashraf, P. Champagne, A. Perwuelz, C. Campagne, A. Leriche, Photocatalytic solution discoloration and self-cleaning by polyester fabric functionalized with ZnO nanorods, Journal of Industrial Textiles. 44 (2015) 884–898, https://doi.org/10.1177/1528083713519662.
[69] A. Hatamie, A. Khan, M. Golabi, A.P.F. Turner, V. Beni, W.C. Mak, A. Sadollahkhani, H. Alnoor, B. Zargar, S. Bano, O. Nur, M. Willander, Zinc Oxide Nanostructure-Modified Textile and Its Application to Biosensing, Photocatalysis, and as Antibacterial Material, Langmuir. 31 (2015) 10913–10921, https://doi.org/10.1021/acs.langmuir.5b02341.
[70] S. Nourbakhsh, M. Montazer, Z. Khandaghabadi, Zinc oxide nano particles coating on polyester fabric functionalized through alkali treatment, Journal of Industrial Textiles. 47 (2018) 1006–1023, https://doi.org/10.1177/1528083716657819.